Transient Solution of an Incompressible Viscous Flow in a Channel with Sudden Expansion/Contraction

Durga C. Dalal, Swapan K. Pandit

Abstract—In this paper, a numerical study has been made to analyze the transient 2-D flows of a viscous incompressible fluid through channels with forward or backward constriction. Problems addressed include flow through sudden contraction and sudden expansion channel geometries with rounded and increasingly sharp reentrant corner. In both the cases, numerical results are presented for the separation and reattachment points, streamlines, vorticity and flow patterns. A fourth order accurate compact scheme has been employed to efficiently capture steady state solutions of the governing equations. It appears from our study that sharpness of the throat in the channel is one of the important parameters to control the strength and size of the separation zone without modifying the general flow patterns. The comparison between the two cases shows that the upstream geometry plays a significant role on vortex growth dynamics.

Keywords—Forward and backward constriction, HOC scheme, Incompressible viscous flows, Separation and reattachment points.

I. INTRODUCTION

IN recent years, there has been considerable interest to study the flow in presence of obstructions such as different types of blocking or various constrictions like a valve, an orifice and so on (which are widely used in a pipe line systems) as these sites are prone to accumulate high shear stress and causes the flow disturbances whose outcome could be important in physiological studies. Further, a reduction in cross sectional area caused by constriction brings about an increase in flow resistance. The dependency of resistance on the flow rate is an important factor for a design of pumping devices. The flow phenomena associated with these problems could be resembled with flow through a channel with forward and backward constricted channel with re-entrant corner. This is a classic problem which is important in both engineering and biomechanics. The richness and complexity of the flow patterns occur in both the cases even in a relatively simplest of geometrical settings. Extensive studies have been performed for flow through asymmetric and symmetric channel with sudden expansion or contraction over the last two decades, which include uniform, non-uniform and pseudospectral grids. The backward facing step flow with right angled expansion asymmetrical geometries possesses a large in number. Among them we can cite Armaly et al. [1], Durst et al. [2], Tutty and Peddly [3] whereas slope with 45^0 and right angled expansion has been studied by Sobey [4].

They made great contributions in the area of channel flow. For the case of flow in a symmetric channel with right angle as well as 45^0 expansion have been studied both experimentally and numerically with different expansion ratio. Among them Durst group [2], [5]-[7], Sobey [4], [8] were prolific contributors. In their studies, the appearance of asymmetric flow with increase in Reynolds number in a symmetrical channel has been justified. This phenomenon is explained by Coanda effect [9] and the causes of instability have been analyzed in [8], [10], [11]. They made a significant stride towards understanding the channel flow with expansion. In the case of oscillatory flow, they have observed a train of vortices in the downstream side of the corner. These flow phenomena were absent in the study of Pedrizzetti [12] in which he has used a circular conduit having smooth rounded corner for the experimental results and numerical predictions. Only when the expansion is sharp, the symmetric jet flow is observed [8]. The study of flow in a channel with different degree of constriction in a channel with forward and backward constriction is limited [13], [14] which motivates to determine the flow restrictive effects of the geometry having the reentrant corner with different curvature to meet the purpose of this paper.

In this paper, the flow through axisymmetric non-uniform rigid channel having varying degree of constriction in a forward constriction and backward constriction are discussed numerically over a large range of Reynolds numbers. The present paper is in conjunction with our previous work focusing on the transient flow analysis and the robustness of our proposed scheme [15]. The N-S equations in stream-function vorticity form were solved using our proposed fully implicit HOC scheme which is second or first order accurate in time depending on a weighted average parameter and fourth order accurate in space. For choice of the value 0.5 of the weighted average parameter gives rise to a second order Crank-Nicholson type scheme which we have used in our computations. Detailed scheme can be found in [15].

The paper is organized in the following way: section 2 describes the numerical procedure, section 3 presents and discusses the details numerical results, and Section 4, the conclusion.

II. MATHEMATICAL FORMULATIONS

A. Governing Equations

The governing equations representing the 2-D unsteady incompressible viscous flow of a fluid are the N-S equations which, in non-dimensional primitive variable formulation can be written as

$$\frac{\partial u}{\partial x} + \frac{\partial v}{\partial y} = 0, \tag{1}$$

D. C. Dalal is with Indian Institute of Technology Guwahati, Guwahati 781039, India (phone: +91-361-258-2615; fax: +91-361-258-2649; e-mail: durga@iitg.ernet.in).

S. K. Pandit is Visva-Bharati, Santiniketan 731235, India. (e-mail: swapankumar.pandit@visva-bharati.ac.in).

$$\frac{\partial u}{\partial t} + u\frac{\partial u}{\partial x} + v\frac{\partial u}{\partial y} = -\frac{\partial p}{\partial x} + \frac{1}{\text{Re}}\nabla^2 u, \tag{2}$$

$$\frac{\partial v}{\partial t} + u\frac{\partial v}{\partial x} + v\frac{\partial v}{\partial y} = -\frac{\partial p}{\partial y} + \frac{1}{\text{Re}}\nabla^2 v, \tag{3}$$

For non-dimensionalization, we have considered is

$$x^* = \frac{x}{L}, \; y^* = \frac{y}{L}, \; u^* = \frac{u}{u_0}, \; v^* = \frac{v}{u_0}, \; t^* = \frac{t\,u_0}{L},$$

$$p^* = \frac{p}{\rho\,u_0^2}, \; \text{Re} = \frac{L\,u_0}{\upsilon}, \text{ is called Reynolds number, where } L$$

is the unperturbed channel width, u_0 is the average velocity at the entrance and υ is the kinematic viscosity. For convenience, the asterisk sign has been removed from the variables of equations (1)-(3).

Instead of pressure and velocity, the derived quantities such as stream function $\psi(x,y,t)$ and vorticity $\zeta(x,y,t)$ can be defined in terms of u,v as

$$u = \frac{\partial\psi}{\partial y}, \; v = -\frac{\partial\psi}{\partial x} \tag{4}$$

and $\quad \zeta = \frac{\partial v}{\partial x} - \frac{\partial u}{\partial y}. \tag{5}$

With these, the stream function-vorticity $(\psi - \zeta)$ form of the N-S equations (1)-(3) can be written as

$$-\frac{\partial^2\psi}{\partial x^2} - \frac{\partial^2\psi}{\partial y^2} = \zeta, \tag{6}$$

$$\text{Re}\frac{\partial\zeta}{\partial t} - \frac{\partial^2\zeta}{\partial x^2} - \frac{\partial^2\zeta}{\partial y^2} + u\,\text{Re}\frac{\partial\zeta}{\partial x} + v\,\text{Re}\frac{\partial\zeta}{\partial y} = 0. \tag{7}$$

The equations (6) and (7) are solved for the whole channel width as well as for half width with a symmetry condition on the centerline.

This stream function-vorticity formulation has major advantages over the primitive variable form: firstly, it satisfies the continuity equation automatically and secondly, it decouples the pressure calculation from the velocity calculation. In the process, it also eliminates two computational difficulties, namely, finding (i) the correct boundary condition for pressure, and (ii) an explicit pressure equation satisfying the incompressibility constraint.

B. Flow Geometry and Mesh Structure

In this paper, the numerical study is presented for two test cases. The first one is the forward constricted channel and the second one is a backward constricted channel, formed in a process of contraction and expansion respectively having reentrant corner in both cases. The schematic flow diagrams and corresponding boundary conditions are shown in Figs. 1(a) and 1(b). To resolve the flow accurately at corners, a more refined grid needs to be incorporated. One such mesh structure is provided through a conformal transformation [13]
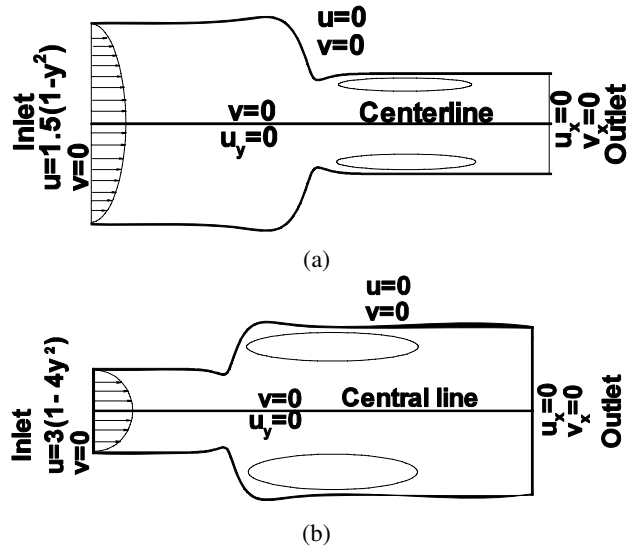

Fig. 1 (a) Forward (physical) (b) backward (physical) constricted channel flow configuration with boundary conditions

that maps the actual nonuniform geometry (physical domain) to a uniform rectangular geometry (computational domain) of width (d) as follows:

$$z = \zeta(A + B\tanh(w)), \tag{8}$$

where $z = x + iy$ and $w = \xi + i\eta \; (i = \sqrt{-1})$ with

$$x = A\xi + \frac{B}{H}[\xi\sinh(2\xi) - \eta\sin(2\eta)], \tag{9}$$

$$y = A\eta + \frac{B}{H}[\eta\sinh(2\xi) + \xi\sin(2\eta)]. \tag{10}$$

Here $H = \cosh(2\xi) + \cos(2\eta)$; A and B are the constants defined by $A = \frac{r_o + r_i}{2\lambda}, B = \frac{r_o - r_i}{2\lambda}$ where r_i, r_o respectively are the inlet and outlet radii of the channel and λ controls the smoothness as well as degree of sharpness of the constriction with increasing value of λ indicating a more sharp corner. In the present computation, in the physical plane the inlet and the outlet radii are taken as $r_i = 1.0$ and $r_o = 0.5$ for forward constricted (Fig. 1(a)) and $r_i = 0.5$ and $r_o = 1.0$ for backward constricted (Fig. 1(b)) channel whereas in the computational plane the width (d) of the channel is taken as λ The corresponding mesh distributions in the physical plane has been cited in Figs. 2(a) and 2(b) for forward and backward constricted channel respectively whereas the varying shape of the top boundary due to different choice of the degree of sharpness of the constriction has been shown in Fig. 3. It is seen that in the first case and second case, $\lambda = 0.6$ makes a smooth gradual contraction and expansion respectively

step-down-constricted channel mesh (physical)

(a)

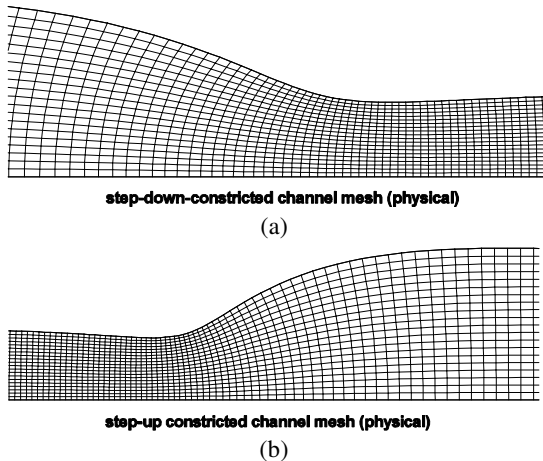step-up constricted channel mesh (physical)

(b)

Fig. 2 Mesh-geometry in the physical plane for (a) forward (b) backward constricted channel
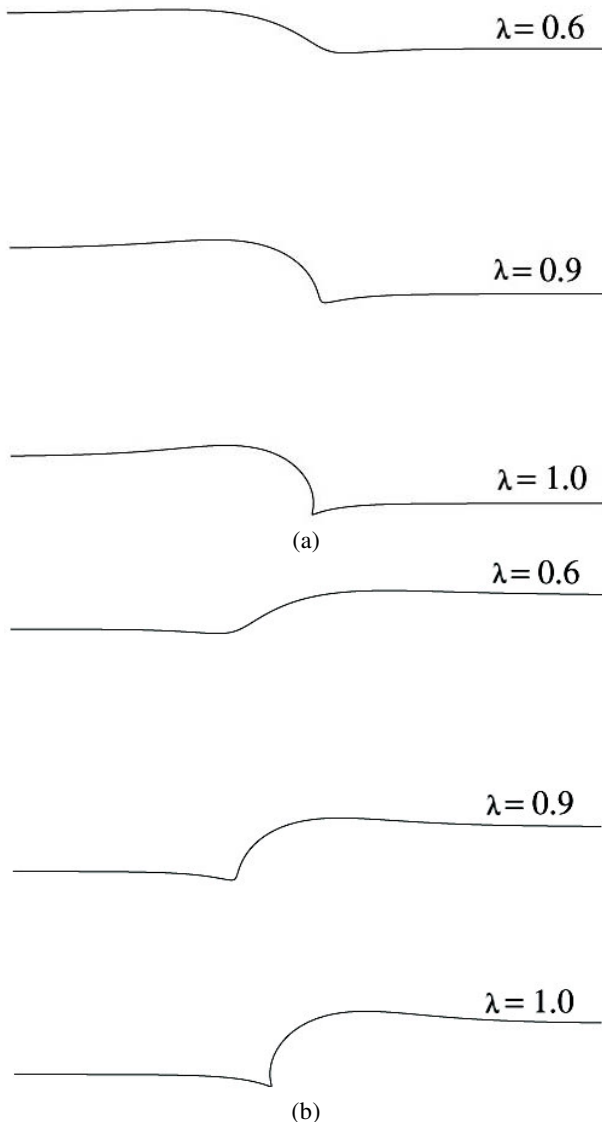

Fig. 3 Top boundary for different degree of constriction in (a) forward (b) backward constricted channel

Whereas $\lambda = 1.0$ produces a severe sharp corner by increasing the height just immediate before and after the corner in comparison to $\lambda = 0.9$. The location of the corner in the forward constricted channel is on the right of origin whereas in the backward constricted channel it appears on the left of origin. Further, in the case of forward and backward constricted channel the sharp edge is in the inward direction of the expanded region.

C. Boundary Conditions

The boundary conditions imposed on the flow domain are as follows:

For whole channel, on the top and bottom wall in both the cases a fixed rigid wall is considered and the usual no-slip condition is imposed i.e.

$$u = v = 0. \tag{11}$$

For half channel, symmetry conditions are upheld on the centerline which translates the radial velocity component and the shear stresses as

$$\frac{\partial u}{\partial y} = v = 0. \tag{12}$$

At the entrance, a parabolic velocity profile is prescribed:

$$u = c_1\left(1 - c_2 \, y^2\right), \; v = 0, \tag{13}$$

where c_1 and c_2 are constants.

At the outlet fully developed flow is considered. A fifth order discrete formula of boundary conditions for u, v, ψ, ζ at the outlet and also for u along the centerline has been employed. The formula is given as follows [16]:

$$T_{i,j} = 0.04\left[48T_{i,j+1} - 36T_{i,j+2} + 16T_{i,j+3} - 3T_{i,j+4} \right.$$

$$\left. - 12h\left(\frac{\partial T}{\partial y}\right)_{i,j+4} \right] + O\left(h^5\right).$$

D. Numerical Procedure

A uniform rectangular mesh of steps h and k is constructed on the computational plane along the ξ and η -directions respectively (Fig. 4). Using central difference formula in the discretization procedure and approximates the higher order derivatives in the truncation error terms by using original equations, together with Crank-Nicholson type scheme for temporal part produces a higher order compact scheme which is fourth order accurate in space and second order accurate in time. This process produces a system of equations in both ψ and ζ.
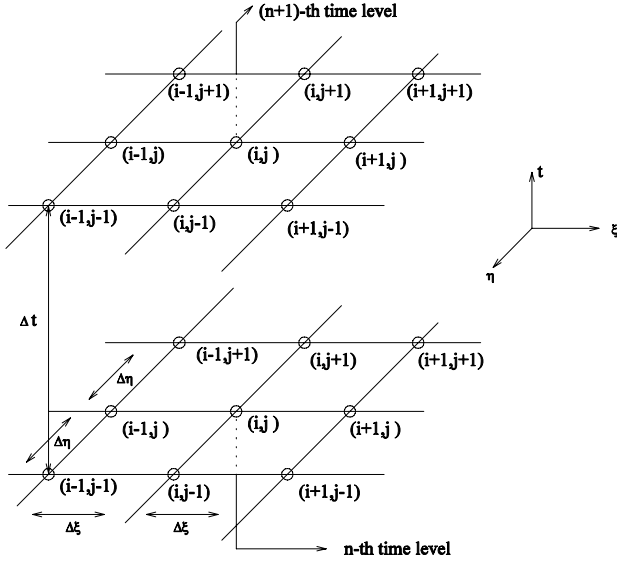
Fig. 4 The 9-point HOC Stencil

The system of equations in ψ, ζ which are obtained after discretization in the transformed plane, can be written in matrix form as

$$A\mathbf{\Phi}^{n+1} = \mathbf{f}\left(\mathbf{\Phi}^{n}\right), \qquad (14)$$

where the coefficient matrix A is an asymmetric sparse matrix. This linear system is, with the present choice of coordinates, made of nine diagonals and non symmetric. For a grid of size $m \times n$, A has dimension mn, and $\mathbf{\Phi}^{n+1}$ and $\mathbf{f}\left(\mathbf{\Phi}^{n}\right)$ are mn-component vectors. As the coefficient matrix A is not generally diagonally dominant, conventional iterative methods such as Gauss-Seidel cannot be used. On uniform grids, some of the associated matrices are symmetric and positive definite, which allows algorithms like conjugate-gradient (CG) [17] to be used. As non-uniform grid invariably leads to non-symmetric matrices, in order to solve these systems the biconjugate gradient stabilized method (BiCGStab) [17], [18], [19] is used here without preconditioning. The convergence criterion for steady state solution is that for all the grid points

$$\max\left|\mathbf{\Phi}^{n+1} - \mathbf{\Phi}^{n}\right| < Tol, \qquad (15)$$

where Tol is the tolerance limit for convergence. The numerical algorithm is as follows:

1) *Accuracy:* In addition to grid step and the tolerance of the iterative procedure, the positions of upstream and the downstream boundaries affect the accuracy of the numerical solution. We have numerically experimented and found that the minimum inlet distance from the throat should be $x \approx -8$ and -10 for forward and backward constricted channel respectively. In order to get a fully developed flow at the outlet for Reynolds numbers up to $Re = 1000$ (for $\lambda = 0.6$), $Re = 750$ (for $\lambda = 0.9$) and $Re = 500$ (for $\lambda = 1.0$), we set

a distance for the outlet condition from the throat as $x \approx 25$ in the case of forward constricted channel whereas for backward constricted channel we set the distance as $x \approx 45$ for Reynolds numbers up to $Re = 500$ (for $\lambda = 0.6$), and $x \approx 30$ up to $Re = 250$ (for $\lambda = 0.9, 1.0$). However, these distances depend on the parameters (Re and width of the channel). Throughout the computation we have used step length $h = \frac{1}{20}, \frac{1}{25}, \frac{1}{30}, \frac{1}{40}$ along the horizontal and $k = \frac{1}{30}, \frac{1}{40}$ along the vertical direction in the computational plane for the corner flow geometry defined by $\lambda = 0.6, 0.9, 1.0$ and time step $\Delta t = 0.001$ in all the cases.

III. RESULTS AND DISCUSSIONS

A. General Flow Behavior

Generally, flows in an axisymmetric constricted channel develop closed separation bubbles (also called as recirculation zones) immediate after the channel throat for relatively large values of Re. In addition to the appearance of vortices, some more complex flow phenomena are usually seen in the case of transient flows, which is not the case for steady flows. Locating the centers of such vortices is difficult from the vorticity field since there is no unique relation between vorticity contours and separated recirculating zones.

The strength of a vortex is defined by the difference between the Max (ψ) in the calculated region and ψ at the wall, and its center is defined by the point at which ψ attains its maximum value. Besides the formation of a strong vortex there exists a large velocity gradient in the flow field, this combination could cause several factors. Therefore, it is important to study the strength and location of a vortex.

In the following two subsections, we have presented results of numerical solutions of the N-S equations for an unsteady flow in a non-uniform rigid channel with a forward constriction and backward constriction having a smooth corner with increasing sharpness. Extensive set of model cases have been considered to study the numerical and physical aspects of the flow.

TABLE I
GEOMETRIES OF FORWARD CONSTRICTED CHANNEL AND REYNOLDS NUMBER RANGE STUDIES

Model	Degree of constriction (λ)	Reynolds number range for calculations	Computed separation Reynolds number
M_1	0.6	1-1000	no separation
M_2	0.9	1-750	168.0
M_3	1.0	1-500	any Re

B. Flow in a Channel with Forward Constriction

In this section, numerical study of flows in an axisymmetric channel with forward constriction has been presented. Numerical results are compared with that of Mancera et al. [13], [14] and they are in excellent agreement. Three model cases have been considered as given in Table I.

We have restricted our study up to $Re = 1000$. The channel geometries used in [13], [14] are closely

approximated by our models given in Table I. It should be mentioned that convergent solutions can be obtained for all the models over a wide range of Reynolds numbers. Time marching steady state results with zero initial condition have been presented in the form of tables (Tables III and IV) as well as in the form of figures (Figs. 5 - 9). A description of the various possible steady state laminar flow patterns is perhaps best rendered by a display of streamlines and vorticity contours for different degrees of constrictions as well as flow parameters.

It has been numerically experimented that no separation zone is formed in the range of the Reynolds numbers studied (given in Table I) for model M_1 ($\lambda = 0.6$), whereas in model M_2 ($\lambda = 0.9$) separation starts to occur at approximately $Re = 168$ and in the case of model M_3 ($\lambda = 1.0$) separation is seen for Reynolds number as low as 1. In the forward constricted channel geometry, separation occurs when $\lambda \geq 0.8$.
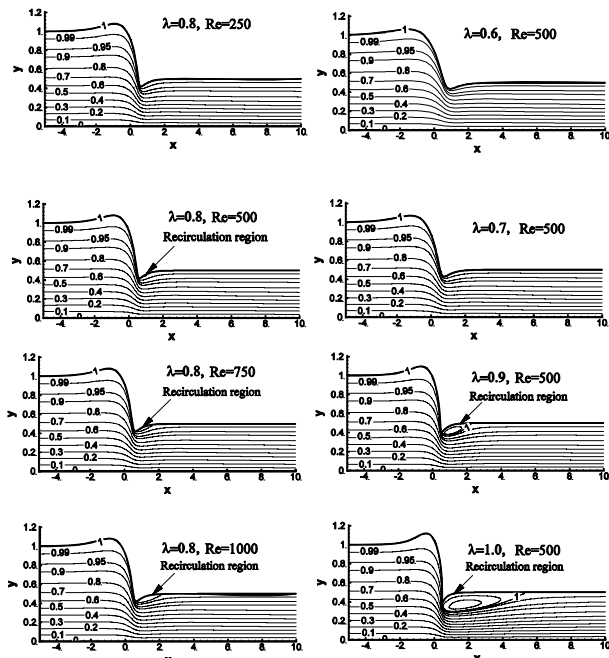

Fig. 5 In a forward constricted channel: The first column corresponds to streamline contour for fixed $\lambda = 0.8$ with different Re and the second column corresponds to streamline contour for Re=500 with different λ.

In Fig. 5, the first column illustrates the curves of constant stream function for a fixed λ ($\lambda = 0.8$) with different Re values and the second column represents the same for a fixed Re with different degrees of constrictions. It is evident that there is no separation zone even for $Re = 500$ in the geometry defined by $\lambda = 0.6, 0.7$ respectively whereas a small recirculation zone develops in the case of $\lambda = 0.8$. It is also seen that in the case of $\lambda = 0.8$, even for higher Res (e.g. $Re = 700, 1000$) the size of the recirculation region is small

compared to lower Re (e.g. $Re = 500$) in the case of model M_2 ($\lambda = 0.9$) and M_3 ($\lambda = 1.0$). The above facts conclude that the corner sharpness is more important for the development of corner vortex than velocity (or Re). In Fig. 6, we have presented the corresponding vorticity contours for Fig. 5. It shows the existence of several high gradient regions in the downstream side of the throat. It can be emphasized that changes in area around the throat of the channel due to different degrees of sharpness could be the main reason for the flow disturbance and the generation of different size of vortices.
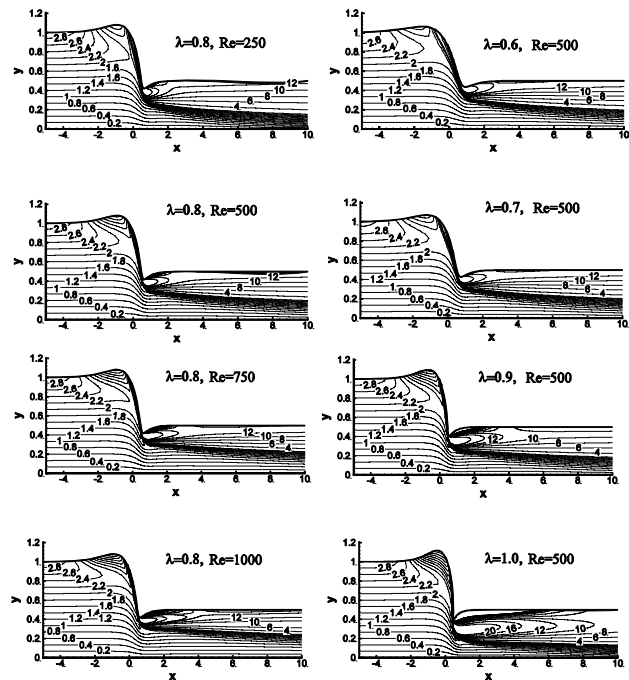

Fig. 6 In a forward constricted channel: The first column corresponds to vorticity contour for fixed $\lambda = 0.8$ with different Re and the second column corresponds to vorticity contour for Re=500 with different λ.

Separation and reattachment points for different Res are presented in the Table II for $\lambda = 0.9$ and $\lambda = 1.0$ respectively. For $Re = 250$ in the case of $\lambda = 1.0$, we have compared our results with [13] (given in Table II) and an excellent agreement has been found. It is seen that the length of the separation zone increases with the increase in Res for both the model cases. In comparison to Table III, it is also seen that in the case of model M_2 ($\lambda = 0.9$), the separation point occurs in the downstream side of the corner for Re as large as 500 but for higher Re (say $Re = 750$) separation point occurs just immediate before the corner whereas in the case of model M_3 ($\lambda = 1.0$), the separation point starts to occur at corner for $250 \leq Re \leq 500$.

TABLE II
SEPARATION AND REATTACHMENT POINTS IN THE FORWARD CONSTRICTED CHANNEL FLOW FOR $\lambda = 0.9$

λ	Re	Separation points (x,y)	Reattachment points (x,y)
0.9	170	(0.65909, 0.42473)	(0.87626, 0.45733)
	250	(0.57916, 0.41010)	(1.25243, 0.485207)
	500	(0.53085, 0.40407)	(2.25000, 0.49930)
	750	(0.51741, 0.40409)	(3.33335, 0.49997)
1.0	50	(0.51349, 0.40068)	(0.64651, 0.43568)
	100	(0.46394, 0.38384)	(1.17478, 0.48834)
	250	(0.45065, 0.38158)	(2.64998, 0.49993)
		(0.456, 0.383)[13]	(2.55, 0.499)[13]
	500	(0.45065, 0.38158)	(5.27500, 0.50000)

TABLE III
LOCATION OF THE CORNER (x_{min}, y_{min}) IN THE FORWARD CONSTRICTED CHANNEL FOR DIFFERENT λ

λ	(x_{min}, y_{min})
0.6	(0.940104, 0.436011)
0.7	(0.750907, 0.428928)
0.8	(0.635091, 0.418853)
0.9	(0.530827, 0.404055)
1.0	(0.450649, 0.381584)

TABLE IV
VORTEX CENTER OF THE FORWARD CONSTRICTED CHANNEL FLOW
FOR $\lambda = 0.9, 1.0$

λ	Re	Vortex center (x,y)	Max(ψ)
0.9	250	(0.8283, 0.4258)	1.00085
	500	(1.1198, 0.4105)	1.00896
	750	(1.4326, 0.4084)	1.01778
1.0	100	(0.6759, 0.3964)	1.00381
	250	(1.0674, 0.3684)	1.02781
	500	(1.6519, 0.3645)	1.04359

In Table IV, the center of the vorticity and its strength have been presented for different Res with different degrees of constriction. It reveals that for a fixed Re the center of the vortex shifts in the downstream with the increase in degree of constriction and the same phenomena occurs for a fixed λ with increase in Re.

Fig. 7 shows the variation of centerline velocity with axial location for the model M_2 ($\lambda = 0.9$) and M_3 ($\lambda = 1.0$) for different Res. It can be seen that the occurrence of peak velocity slightly shifts towards the downstream from its previous position with the increase of Res. Since there is no reliable experimental method to determine wall shear-stress near the recirculation zone, we try to get some information about wall shear stress (wall-vorticity value) theoretically.
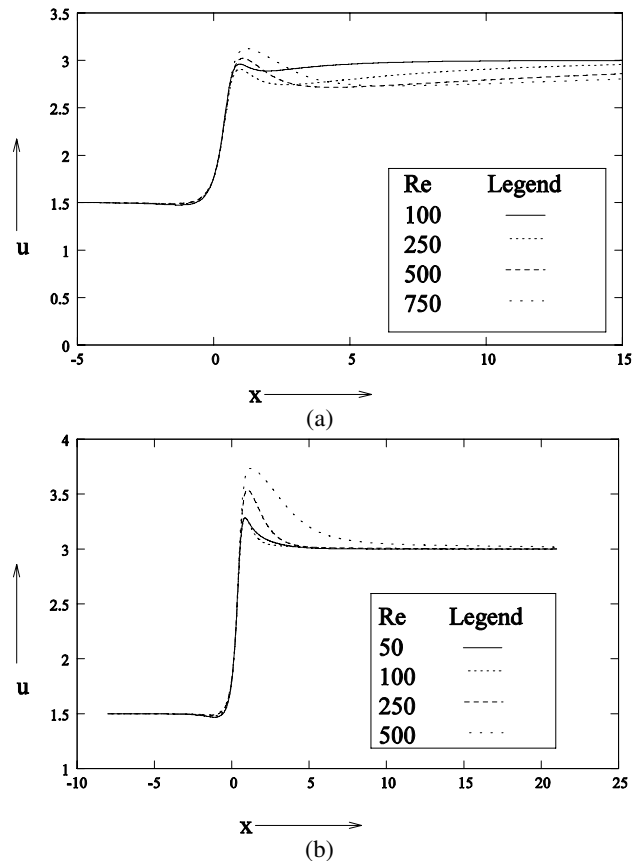

Fig. 7 In a forward constricted channel: Centerline axial velocity for (a) $\lambda = 0.9$ (b) $\lambda = 1.0$

Fig. 8(a) shows the changes in wall vorticity along the x-direction for different Res in the case of model M_1($\lambda = 0.6$). It can be mentioned that no separation region has been noticed even for Re as large as 1000. As Re increases the peak shear stress shifts slowly towards upstream. But in the case of model M_3 ($\lambda = 1.0$) (can be seen in Fig. 8(b)), the peak shear stress occurs at the same point even with increase in Re. In addition to this it is seen that the region of recirculation also increases with increase in Re (which is evident from the negative values of shear stress). That is a central jet, issued from the constriction, creates a potential core bounded by a shear layer which links up to the wall by a recirculation zone. The rapid increase in wall vorticity with Re for the sharp constriction is quite apparent.

Fig. 9 shows the vector plots of the flow field. A parabolic flow was prescribed at the inlet. As soon as it reaches the throat of the constriction, the flow profile is changed to a blunt shaped non-parabolic profile with a negative flow zone near the wall. Figure also reveals that the profile slowly regains the parabolic shape as it moves along the downstream. The negative velocity near the wall indicates the existence of separation zone.
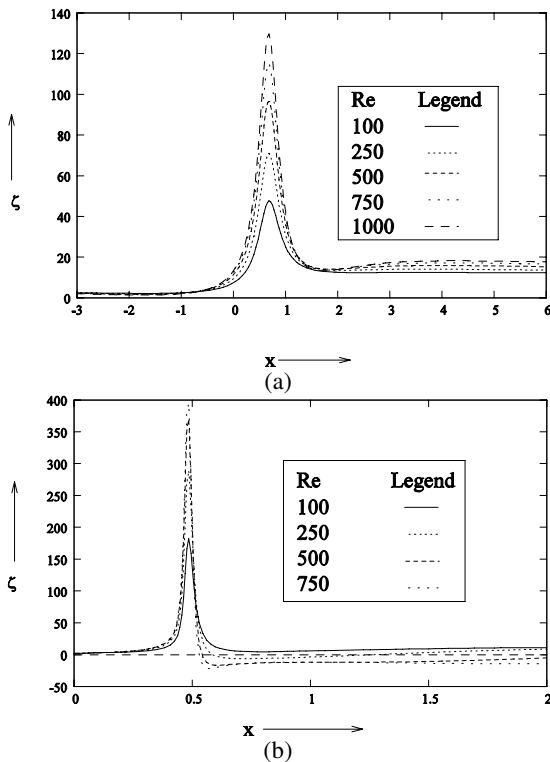
(a)

(b)

Fig. 8 Wall vorticity for (a) $\lambda = 0.6$ (b) $\lambda = 0.9$ in a forward constricted channel
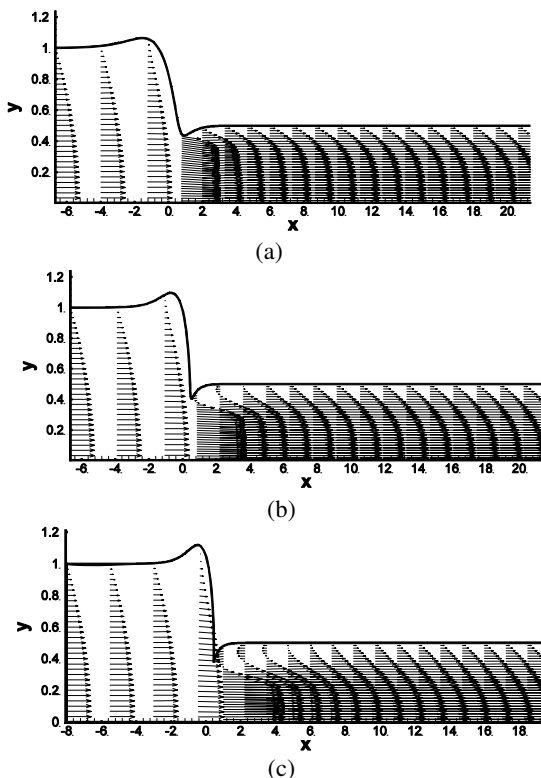

(a)

(b)

(c)

Fig. 9 Velocity Profile for (a) $\lambda = 0.6$, Re=1000 (b) $\lambda = 0.9$, Re=750 (c) $\lambda = 1.0$, Re=500 in a forward constricted channel

C. Flow in a Channel with Backward Constriction

Numerical results for flow in a channel with backward constriction have been presented in this section. The degree of sharpness of the corner has been considered same as in the case of forward constricted channel. Table V shows the range of Reynolds numbers studied and the critical Res for flow separation for different values of λ (called as model m_1, m_2, m_3).

TABLE V
GEOMETRIES OF BACKWARD CONSTRICTED CHANNEL AND REYNOLDS NUMBER RANGE STUDIES

Model	λ	Reynolds number range for calculations	Computed separation Reynolds number
m_1	0.6	1-500	15.0
m_2	0.9	1-250	4.0
m_3	1.0	1-250	any Re

TABLE VI
VORTEX CENTER OF THE BACKWARD CONSTRICTED CHANNEL FLOW FOR
$\lambda = 0.6, 0.9, 1.0$

λ	Re	Vortex center (x,y)	Max(ψ)
0.6	50	(1.0697, 0.7319)	1.0310
	100	(1.7848, 0.7035)	1.0556
	250	(3.0080, 0.6450)	1.0687
0.9	50	(0.9178, 0.6716)	1.0871
	100	(1.4778, 0.6428)	1.0966
	250	(3.0330, 0.6162)	1.0929
1.0	50	(0.8919, 0.6383)	1.1208
	100	(1.4081, 0.6030)	1.1214
	250	(3.5194, 0.6013)	1.1125

Table VI shows the vortex center and the maximum value of ψ for all three model cases. It is seen from this table that in each model the center of the vortex moves towards downstream with the increase in Re. For lower Re, degree of constriction becomes responsible for shifting the vortex center towards upstream whereas for higher Re, flow velocity becomes more important than degree of constriction in moving the center towards downstream which can also be observed from Figs. 9 and 17.

TABLE VII
SEPARATION AND REATTACHMENT POINTS FOR THE BACKWARD CONSTRICTED CHANNEL FLOW FOR $\lambda = 0.6$

λ	Re	Separation points (x,y)	Reattachment points (x,y)
0.6	50	(-0.4940, 0.5600)	(3.5680, 1.0199)
	100	(-0.5677, 0.5186)	(7.2497, 1.0005)
	250	(-0.6188, 0.4939)	(18.6667, 1.0000)
0.9	50	(-0.4728, 0.4317)	(4.2593, 1.0010)
	100	(-0.4777, 0.4239)	(8.5000, 1.0000)
	250	(-0.4857, 0.4151)	(21.6668, 1.0000)
1.0	50	(-0.4478, 0.3829)	(4.7600, 1.0002)
	100	(-0.4479, 0.3829)	(9.4000, 1.0000)
	250	(-0.4478, 0.3829)	(23.2800, 1.0000)

In Table VII, we have presented the separation and reattachment points for all the three model cases. It is seen that for model m_1 ($\lambda = 0.6$) and m_2 ($\lambda = 0.9$), as Re increases the separation point moves slightly towards the upstream and the reattachment point moves towards downstream, whereas for model m_3 ($\lambda = 1.0$) the separation point almost remains unchanged though the reattachment point moves towards downstream, which can be observed from Figs. 10(a), 11(a) and 12(a) respectively. As a result, the large amplitude vortex develops in the downstream side of the corner in all the cases. It is also seen that for model m_1 ($\lambda = 0.6$) a large vortex develops even for Re as small as 50. The increase in area just after the constriction in the case of backward constricted channel flow causes pressure loss which brings out a larger size vortex.
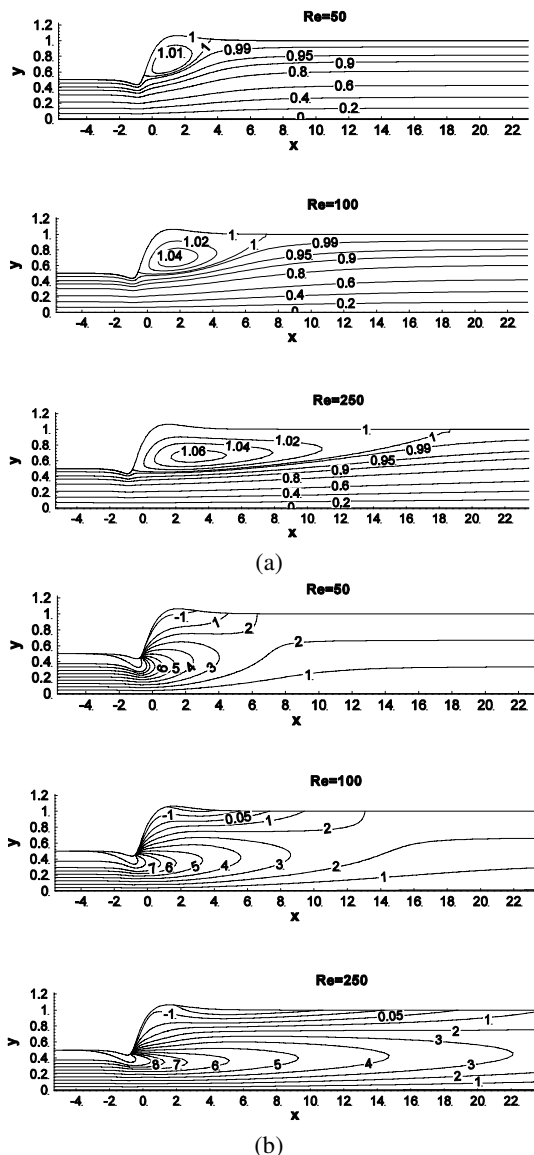
Fig. 10 In a backward constricted channel: (a) Streamline-contours and (b) corresponding vorticity contours for $\lambda = 0.6$.
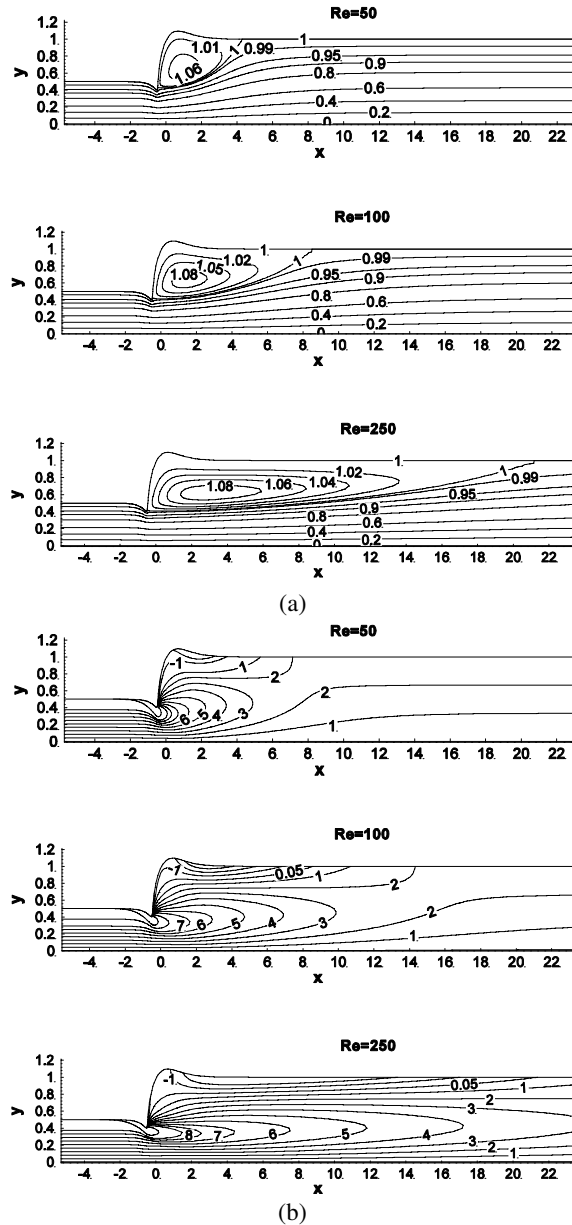

Fig. 11 In a backward constricted channel: (a) Streamline-contours and (b) corresponding vorticity contours for $\lambda = 0.9$.

Figs. 13 and 14 show a time-wise evolution of the streamlines for $Re = 100$ in the case of model m_1 ($\lambda = 0.6$) and m_2 ($\lambda = 0.9$) respectively. For the model m_1 ($\lambda = 0.6$) at $t = 2.5$, there is a small separated region in the downstream of the corner with a strong vortex at $x \approx 1$ (given in Fig. 13). As time evolves the separated region becomes larger with a weaker vortex at $x \approx 2$, which can be seen from the Fig. 13. At $t = 20$, the flow becomes nearly steady by forming a large vortex. On the other hand for the model m_2 ($\lambda = 0.9$), (given in Fig. 14) intermediate flow features become more complicated. The separation region increases gradually with time. At $t = 2.5$, a small separation region evolves with a

strong vortex at $x \approx 0$. As time passes (say $t = 5$ or 10), the vortex grows and splits into a number of smaller vortices. When flow approaches the steady state (say at $t = 20$), these small vortices coalesce and formed a larger separated region. The centerline velocity data have been presented in Fig. 15 for each model with different Res. It shows that for each model the peak of the centerline velocity occurs just immediate after the throat for lower Res and the peak shifts in the downstream with the increase in Re. It is also noticed that in each model for lower Res the centerline velocity decreases sharply up to a small distance along the downstream just after reaching its peak value and then it behaves asymptotically to attain a constant value (for example, it is 1.5 for Re = 50) whereas for higher Res, this decrease is linear from its peak value.
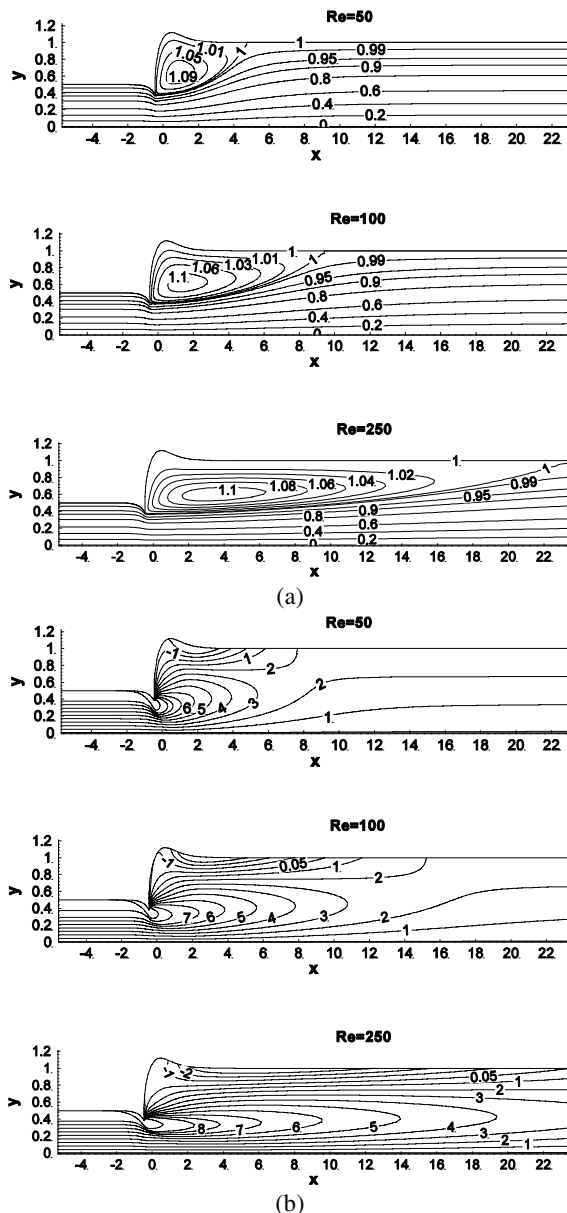

(a)

(b)

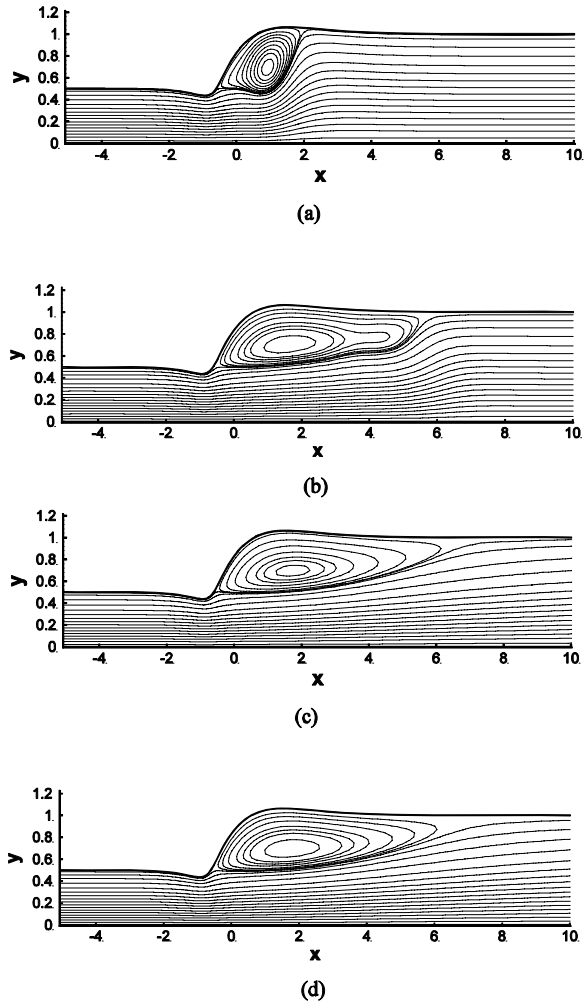Fig. 12 In a backward constricted channel: (a) Streamline-contours and (b) corresponding vorticity contours for $\lambda = 1.0$.

Fig. 13 Time evolution for $\lambda = 0.6$, Re=100 at (a) t=2.5, Max(ψ)=1.13756 (b) t=5.0, Max(ψ)=1.05486 (c) t=10.0, Max(ψ)=1.05534 (d) t=20.0, Max(ψ)=1.05525 in a backward constricted channel

In Fig. 16, we have presented the wall shear stress (wall vorticity) values for each model. For model m_1 ($\lambda = 0.6$) and m_2 ($\lambda = 0.9$) as Re increases the peak shear stress shifts slightly to upstream and it occurs at the onset of the corner whereas for model m_3 ($\lambda = 1.0$) peak shear stress occurs at the same point and it is very near to the corner (given in Fig. 13). It is also noticed that as the degree of constriction increases the wall share stress changes sharply. In addition to this, it is mentioned that the peak values of the wall shear stress increases significantly with the degrees of constriction. As in the case of forward constricted channel, the negative vorticity values in Figs. 16(a), (b), (c) represent the regions of flow separation.
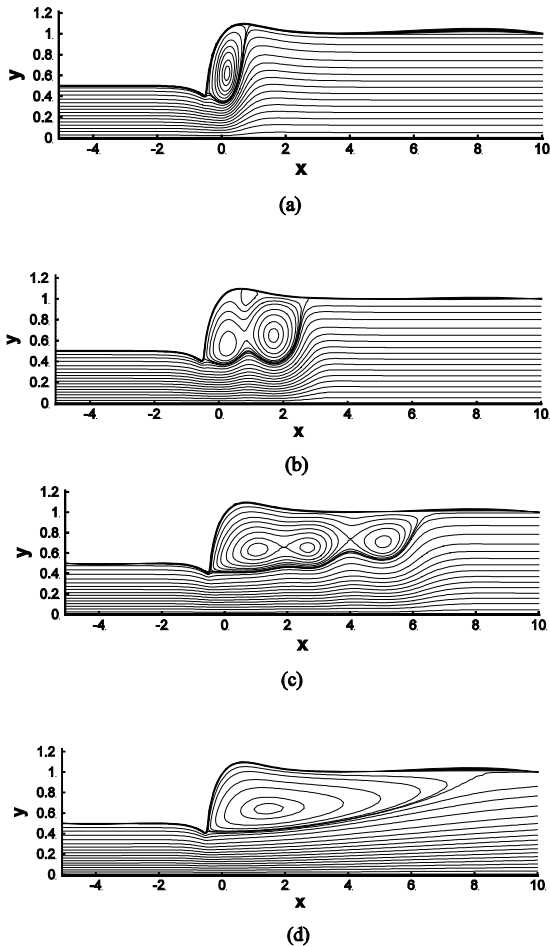
Fig. 14 Time evolution for $\lambda = 0.9$, Re=100 at (a) t=2.5,
Max(ψ)=1.13756 (b) t=5.0, Max(ψ)=1.05486 (c) t=10.0,
Max(ψ)=1.05534 (d) t=20.0, Max(ψ)=1.05525 in a backward
constricted channel

Fig. 17 shows the vector plots of the flow field. A parabolic flow was prescribed at the inlet in this case also. It retains the parabolic shape at the throat with a negative velocity zone in the expansion region. As the profile moves along the downstream, slowly the parabolic part is extended vertically and it reduces the negative flow zone. Finally after some distance negative zone disappears and there is a parabolic velocity profile throughout the channel. In comparison of the flow field in the backward constricted channel with the same in the forward constricted channel, it is noticed that the area of the negative velocity zone i.e separation zone in backward constricted channel is greater than that in the forward constricted channel. It is because of the fact that the flux at the upstream in the backward constricted channel reduces at the throat due to contraction and some amount of fluid flows in the opposite direction but in the case of forward constricted channel the flux at the upstream diffuses in an expanded region after the throat which causes the pressure drop and forms a large separation zone.
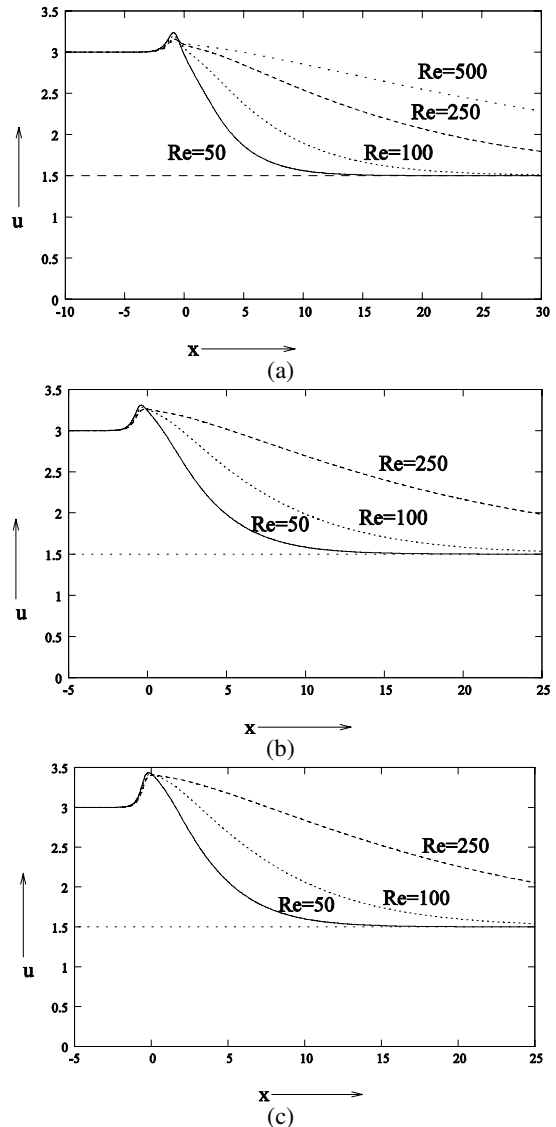

Fig. 15 In a backward constricted channel: Centerline axial velocity
for (a) $\lambda = 0.6$ (b) $\lambda = 0.9$ (c) $\lambda = 1.0$

IV. CONCLUSION

The present work is to study the transient flows in an axisymmetric channel with forward or backward constriction. The governing equations have been solved using higher (fourth) order compact (HOC) scheme. The axial symmetry in the flow pattern has been noticed throughout the channel. Some interesting flow features of this channel flow with forward constriction or backward constriction have been presented in this work. Sharpness of the throat in the channel is one of the important parameters to control the strength and size of the separation zone without modifying the general flow patterns. Generally, flow separation takes place just after the throat at higher values of λ or Re. It can be mentioned that flow separation does not occur for $\lambda \leq 0.7$ even at higher Res
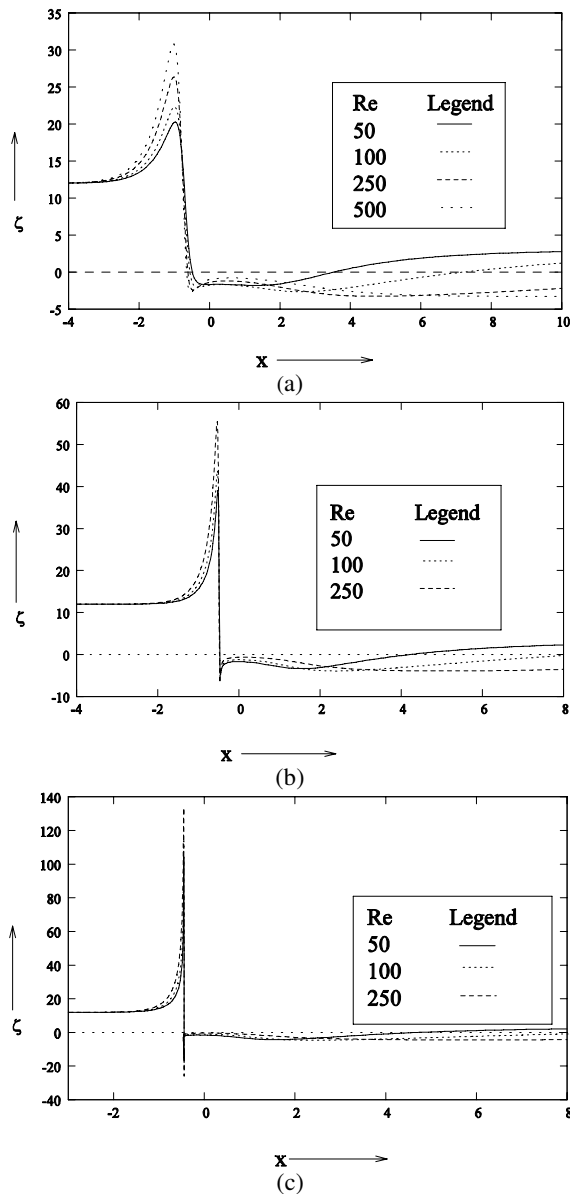
Fig. 16 Wall shear-stress for (a) $\lambda = 0.6$ (b) $\lambda = 0.9$ (c) $\lambda = 1.0$ in a backward constricted channel

Fig. 17 Velocity profile for Re=250 (a) $\lambda = 0.6$ (b) $\lambda = 0.9$ (c) $\lambda = 1.0$ in a backward constricted channel.

Fig. 18 Point of separation and reattachment points in the backward constricted channel geometry defined by $\lambda = 0.6$ for (a) Re=100 (b) Re=250 (c) Re=400.

(say, $Re = 1000$) whereas flow separation has been observed at the throat for $Re = 500$ when $\lambda = 0.8$.

The size of the vortex developed in forward constricted channel flow is small compared to that in backward constricted channel flow. The development of a negative wall shear stress region in the flow through a constricted channel is a common feature. In the case of backward constricted channel there is a sudden change in shear stress values from positive to negative whereas in the case of forward constricted channel this change is smooth. The parabolic flow profile prescribed at the inlet of the forward constricted channel becomes blunt near the throat whereas in the case of backward constricted channel the shape of the inlet profile is maintained.
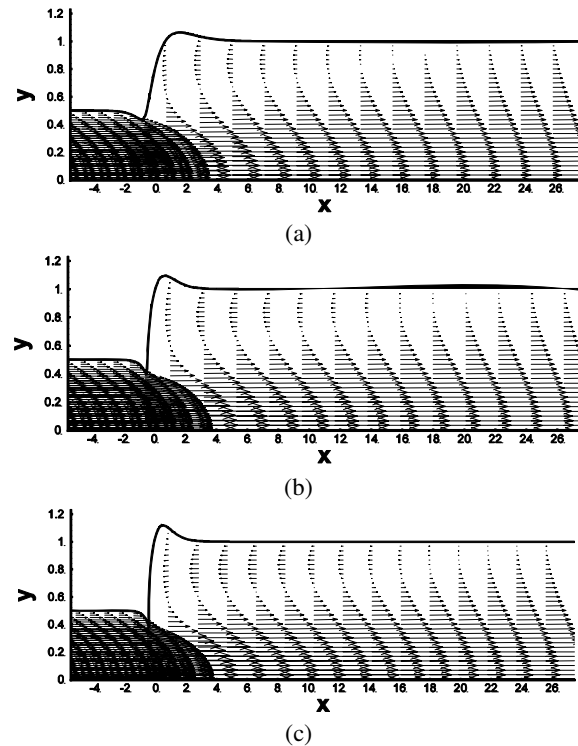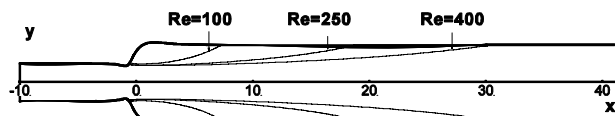
Also in our study, we have shown the axisymmetrical flow behavior in the whole channel for the plane Poiseuille flow (through Fig. 18) which contradicts the some studies of Sobey, Pedley, and Durst group in which they have shown the presence of flow asymmetry in the right angled and 45^0 sloped expansion channel for oscillatory flow with different contraction ratio and supports the results obtained by Pedrizzetti [12]. This difference in flow phenomena may be due to the different flow geometry and inlet flow conditions.

It can be also pointed out that the generation of a series of vortices has not been observed in this study because of axisymmetric flow. The present study enriches various aspects of channel flows and a good opportunity to encompass in details of the flow patterns.

REFERENCES

[1] B. F. Armaly, F. Durst, J. C. F. Pereira and B. Schonung, "Experimental and theoretical investigation of backward-facing step flow," *Journal of Fluid Mechanics*, vol. 127, pp. 473-496, Feb. 1983.

[2] F. Durst, A. Melling and J. H. Whitelaw, "Low Reynolds number flow over a plane symmetrical sudden expansion," *Journal of Fluid Mechanics*, vol. 64, no. 1, pp. 111-128, June 1974.

[3]   O. R. Tutty and T. J. Pedley, "Oscillatory flow in a stepped channel, *Journal of Fluid Mechanics*," vol. 247, pp. 179-204, Feb. 1993.

[4]   I. J. Sobey, "Observation of waves during oscillatory channel flow," *Journal of Fluid Mechanics*, vol. 151, pp. 395-426, Feb. 1985.

[5]   W. Cherdron, F. Durst and J. H. Whitelaw, "Asymmetric flows and instabilities in symmetric ducts with sudden expansions," *Journal of Fluid Mechanics*, vol. 84, no. 1, pp. 13-31, Jan. 1978.

[6]   F. Durst and J. C. F. Pereira, "Time dependent laminar backward-facing step flow in a two dimensional duct," *Trans. ASME: Journal of Fluids Engineering*, vol. 110, no. 3, pp. 289-296, Sept. 1988.

[7]   F. Durst, J. C. F. Pereira and C. Tropea, "The plane symmetric sudden expansion flow at low Reynolds numbers," *Journal of Fluid Mechanics*, vol. 248, pp. 567-581, March 1993.

[8]   I. J. Sobey and P. G. Drazin, "Bifurcations of two dimensional channel flows," *Journal of Fluid Mechanics*, vol. 171, pp. 263-287, Oct. 1986.

[9]   R. Wille, and H. Fernholz, "Report on the first European Mechanics Colloquium on the Coanda effect," *Journal of Fluid Mechanics*, vol. 23, no. 4, pp. 801-819, Dec. 1965.

[10] M. S. Borgas and T. J. Pedley, "Non-uniqueness and bifurcation in annular and planar channel flows," *Journal of Fluid Mechanics*, vol. 214, pp. 229-250, May 1990.

[11] M. Shapira, D. Degani and D. Weihs, "Stability and existence of multiple solutions for viscous flow in suddenly enlarged channels," *Computers and Fluids*, vol. 18, no. 3, pp. 239-258, 1990.

[12] G. Pedrizetti, "Unsteady tube flow over an expansion," *Journal of Fluid Mechanics*, vol. 310, no. 5, pp. 89-111, March 1996.

[13] P. F. A. Mancera and R. Hunt, "Fourth order method for solving the navier-stokes equations in a constricted channel," *International Journal of Numerical Methods in Fluids*, vol 25, no. 11, pp. 1119-1135, June 1997.

[14] P. F. A. Mancera, "A study of numerical solution of the steady two dimensional navier-stokes equations in a constricted channel problem by a compact fourth order method," *Applied Mathematics and Computation*, vol. 146, no. 2-3, pp. 771-790, Dec. 2003.

[15] S. K. Pandit, J. C. Kalita and D. C. Dalal, "A transient higher order compact scheme for incompressible viscous flows on geometries beyond rectangular," *Journal of Computational Physics*, vol. 225, no. 1 pp. 1100-1124, July 2007.

[16] J. C. Tannehill, D. A. Anderson and R. H. Pletcher, *Computational Fluid Mechanics and Heat Transfer*, Hemisphere Publishing Corporation, New York, 1984.

[17] C. T. Kelley, *Iterative methods for Linear and Nonlinear Equations*, SIAM Publications, Philadelphia, 1995.

[18] Y. Saad, *Iterative Methods for Sparse Linear Systems*, PWS Publishing Company, 1996.

[19] H. V. D. Vorst, "BiCGSTAB: A fast and smoothly converging variant of BiCG for the solution of nonsymmetric linear systems," *SIAM J. Sci. Comput.*, vol. 13, no. 2, pp. 631-644, 1992.